Synthesis and Characterization of ZnSe$_{1-x}$Te$_x$ Alloy Thin Films Deposited by Electron Beam Technique

J. Suthagar[1], N.J. Suthan Kissinger[2]

[1] *Department of Physics, Karunya University, Coimbatore-641 114, India*
[2] *Department of Physics, Jubail University College, Jubail Industrial City 31961, Saudi Arabia*

ZnSe$_{1-x}$Te$_x$ solid solutions were prepared and films were deposited on glass substrates with $x = 0.2$, 0.4, 0.6 and 0.8. DTA/TGA analysis was carried out to study the alloy formation temperature. Structural studies by XRD results showed the polycrystalline nature of the films. The Full Width at Half Maximum (FWHM) values were observed from the XRD pattern and used to evaluate the microstructural parameters like crystallite size, strain, dislocation density and stacking fault density for all the films with $x = 0.2$, 0.4, 0.6 and 0.8. These films were coated with a thickness of about 200 nm on glass substrates keeping the temperature constant at 200°C. All films showed cubic structure and the lattice parameter values are found to vary with 'X'. This confirms the solid solution formation between the ZnSe and ZnTe binary compounds which are found to obey Vegard's law. SEM and AFM studies have been arried out to observe their surface modification with solid solution formation. Raman studies confirm the formation of ZnSe$_{1-x}$Te$_x$ compound films.

Keywords: ZnSe$_{1-x}$Te$_x$, ZnSe, ZnTe, Solid Solution, DTA/TGA.

PACS numbers: 73.61.Ga, 68.55.A, 68.60Dv, 61.05.cp

1. INTRODUCTION

Recent technological breakthroughs and the desire for new functions generate an enormous demand for novel materials. ZnSe, ZnTe are the most important materials among II-VI compounds because of its potential applications in the fabrication of blue-green laser, light emitting diodes, photo/electroluminescent displays, dielectric mirrors, optical filters, window layers in heterojunction solar cells and other optically sensitive devices.

Ternary alloys, such as ZnSe$_{1-x}$Te$_x$, are technologically useful because the band-gap can be tuned between the end-member values as the composition, x, is varied. This makes the proper characterization of these materials the subject of much investigation [1-4]. ZnSe$_{1-x}$Te$_x$ is an example of a II-VI semiconductor pseudobinary alloy that can be made over the entire range of compositions [5]. II-VI alloys are becoming increasingly important because they are often used as the basis for magnetic semiconductors with the additional alloying of small amounts of Mn on the metal sublattice [6, 7]. The recent suggestion that high-speed logical circuits can be made out of devices using spin diffusion instead of electron diffusion (so-called "spintronics") is adding extra impetus to research into these materials [8]. Clearly, it is important to be able to characterize the microstructure of these alloys in detail.

Both ZnTe and ZnSe have the zinc-blende structure where the Zn atoms and Te, Se atoms occupy the two interpenetrating face-centered-cubic (fcc) lattices. In the alloys the lattice parameter of ZnSe$_{1-x}$Te$_x$ interpolates linearly between the end member values consistent with Vegard's law. ZnSeTe alloy is a candidate material for blue-green and yellow LDs, since it is lattices matched to GaAs and are expected to have p-dopability [9].

2. EXPERIMENTAL PROCEDURE

2.1 Synthesis of ZnSe$_{1-x}$Te$_x$ alloys materials

Finely powdered samples of ~ 10 g of ZnSe$_{1-x}$Te$_x$ were made with $x = 0.2$, 0.4, 0.6 and 0.8. The starting reagents (zinc selenide, metal basis, 99.9995 %; zinc telluride, metal basis, 99.999 %) were finely ground, mixed in the correct stoichiometry, and sealed in quartz tubes under vacuum. The samples were then heated at 900°C for 12-16 hours. This procedure of grinding, vacuum sealing, and heating was repeated two times to obtain high quality and homogeneous materials. The colors of the solid solutions vary gradually from dark red (ZnTe) to brownish yellow (ZnSe) as the x-value decreases reflecting the band-gap of the alloy samples smoothly changing in the optical frequency range.

2.2 Thin film preparation

Amongst the various techniques available, one of the physical vapour deposition methods of electron beam (EB) evaporation technique is the scarcely used method for the deposition of device quality II-VI thin films, because it affords flexibility in the control over various deposition parameters and easy adaptability of this technique for commercial purposes. EB evaporation technique has been used in the present study, which conqruently will evaporate Zn, Se and Te to get nearly stoichiometric ZnSe$_{1-x}$Te$_x$ alloy films with nano structure.

3. RESULTS AND DISCUSSIONS

3.1 TG/DTA analysis of ZnSe + ZnTe mixed systems

Thermal analysis of ZnSe$_{1-x}$Te$_x$ mixed alloy systems has been carried out to study the behaviors of these binary mixtures to make ternary alloys compounds.

Both these compounds have cubic structure but their melting point is 1523°C and 1295°C for ZnSe and ZnTe respectively. TG/DTA studies may provide information about the staple temperature region upto which they can be deposited as thin films without any disintegration of the respective compounds.

Fig. 1 a, b, c and d show the TG/DTA curves of the mixed compounds $ZnSe_{1-x}Te_x$ with the Te content as x = 0.2, 0.4, 0.6 and 0.8 respectively. From the TG curves it is observed that the weight loss is constant

upto a temperature of 380, 350, 350 and 320°C respectively. Correspondingly, the DTA curves show the position of exothermic peaks at about 437, 464, 457 and $507°$C respectively. Based on these observations, the deposition temperature of the mixed alloy was fixed at $200°$C. It is well below the weight loss starting point temperatures of the mixed compounds.
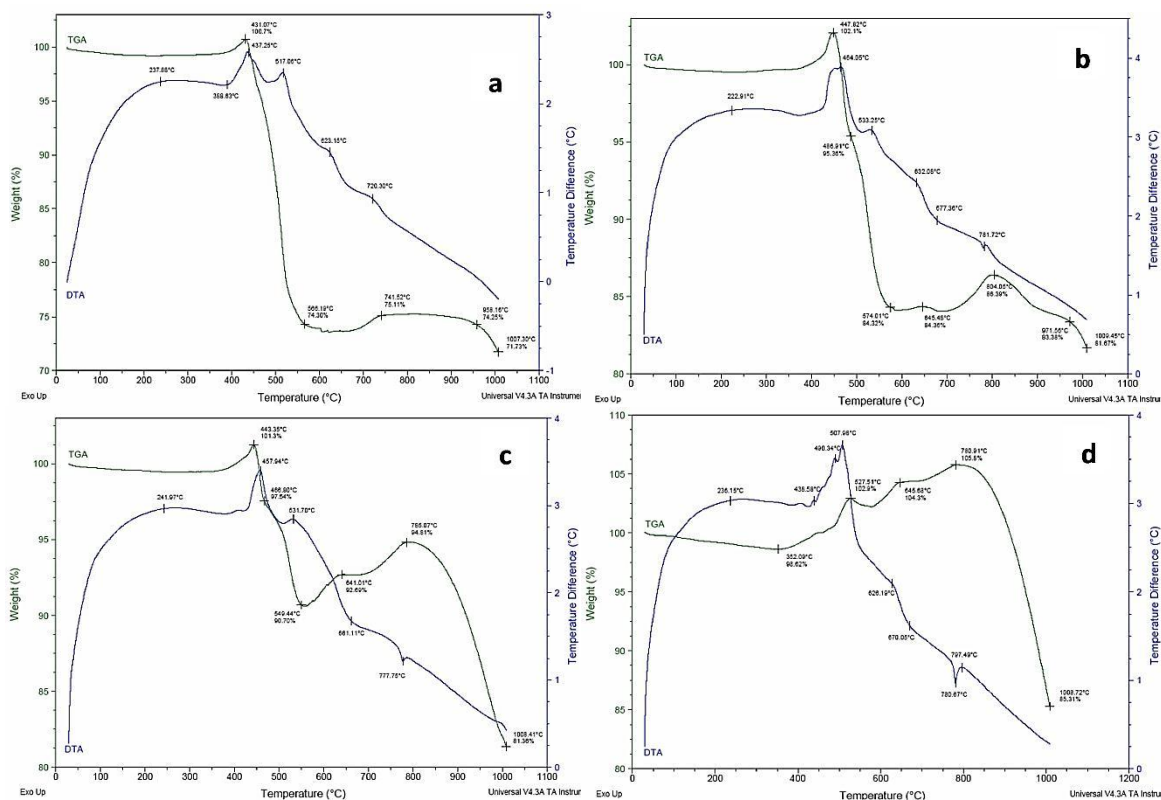

Fig. 1 – TG/DTA curves for the $ZnSe_{1-x}Te_x$ with a) x = 0.2, b) x = 0.4, c) x = 0.6 and d) x = 0.8

3.2 X-ray diffraction

XRD spectra of the EB evaporated $ZnSe_{1-x}Te_x$ with different Te content x = 0.2, 0.4, 0.6 and 0.8 were analysed to study the film nature, phases present and the structure formed. This provides information about the ZnSe base binary material being their lattice modified by the introduction of different ZnTe content. This is attributed to the fact that the atomic radius of Te is 1.405 Å which is larger than that of Se atom of radius 1.255 Å [10].

Fig. 2 a, b, c and d show the XRD patterns of $ZnSe_{1-x}Te_x$ films with various 'X' values equal to 0.2, 0.4, 0.6 and 0.8. The observation of sharp and well defined peak indicates the high crystallized and polycrystalline nature of all films. This well developed and highly intense peak, observed at about $2\theta = 26.51°$, corresponds to (002) reflection. Other peaks are not observed may be due to their very low peak intensities compared to the (002) peak. This reveals the single crystalline orientation nature of the $ZnSe_{1-x}Te_x$ films deposited in this study which confirms the formation of cubic crystalline nature with texturing along (002)

plane. It is observed from the Fig. 2 that the 2θ value is found shifted towards lower angle side with increasing Te content. When the Te content x = 0.8, the '2θ' value is reduced to $25.46°$. This is a definite evidence of deposition of homogeneous and solid solutions of $ZnSe_{1-x}Te_x$ films by using EB evaporation technique.

The presence of only (002) orientation in these films indicates that the crystallites are preferentially oriented with their C-axis perpendicular to the substrate. The lattice space'd' values are found increasing from 3.362 Å to 3.496 Å with increased Te content. Table 1 gives the lattice constant and '2θ' values calculated for the $ZnSe_{1-x}Te_x$ films with x = 0.2, 0.4, 0.6 and 0.8.

The lattice parameter values 'a' was calculated on the assignment of cubic structure for all the $ZnSe_{1-x}Te_x$ films and are given in Table 1. The 'a' values are plotted as a function of 'x' (Te content) as shown in Fig. 3. The value of 'a' is increasing from 0.579 to 0.605 nm with increased Te content. This result confirms the solid solution formation between ZnSe and ZnTe binary compounds to form various ternary alloys. Further, the lattice parameters of these solid solutions are found to obey the Vegard's Law. It means that the lattice con-

stant and the microstructural parameters of $ZnSe_{1-x}Te_x$ ternary alloys can be linearly varied from the starting binary alloy ZnSe [11-13]. These results shows that these ternary alloys have only cubic structure and the

ZnSe - ZnTe compound system produces solid solutions at all 'x' content by one to one substitution of Te atom in the atomic position of 'Se'.
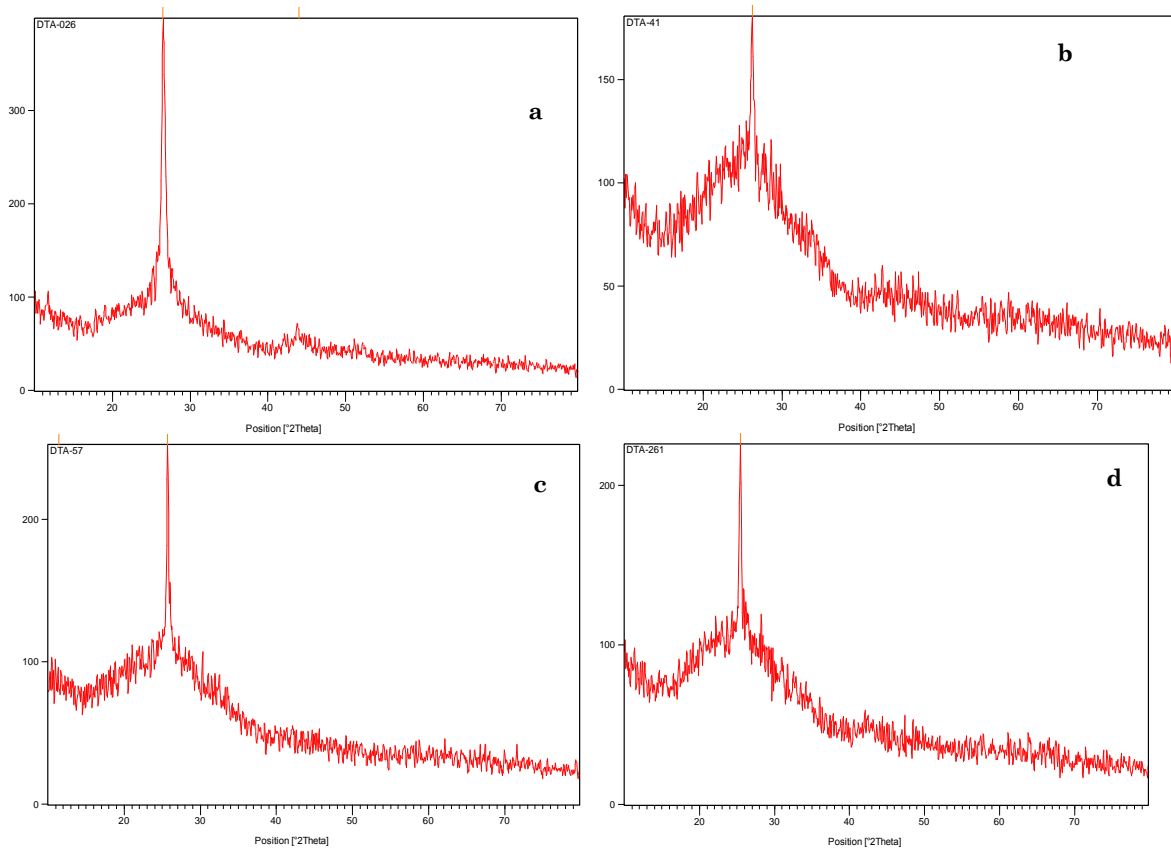

Fig. 2 – XRD patterns for the $ZnSe_{1-x}Te_x$ films with a) $x = 0.2$, b) $x = 0.4$, c) $x = 0.6$ and d) $x = 0.8$

Fig.3 shows the lattice parameters of $ZnSe_{1-x}Te_x$ films as a function of Te content (x). As the Te content increases, the lattice parameter 'a' value increases linearly. The observed 'a' value from the XRD data is given in Fig. 3 a. The interpolated 'a' values using the equation 1 is shown in Fig. 3 b. The 'a' values for the deposited solid solution films are little larger than the interpolated values. However, they are smaller than the 'a' values for the bulk ZnSe (0.5669 nm) and ZnTe (0.6104 nm). This is due to the thermal strain from the thermal expansion difference of ZnSe (7.7×10^{-6} K^{-1}) and ZnTe (8.3×10^{-6} K^{-1}) [14].

Table 2 shows the microstructural parameters of these solid solutions. The grain size is found increasing with enhanced Te content of x = 0.2, 0.4, 0.6 and 0.8. This is obvious due to the fact that Te is anionically substituted at the Se locations and ionic radius of Te is larger (2.21 Å) than that of Se (1.98 Å). Correspondingly, the lattice defects like strain, stress, dislocation density and the number of crystallites all show a decreasing trend with increased Te content.

According to Vegard's law, the value of lattice parameters of alloy semiconductors can be theoretically obtained by interpolation using the equation.

$$ax = F_1 a_1 + F_2 a_2 \qquad (1)$$

where a_1 and a_2 are the lattice parameters of ZnSe

and ZnTe binary componds respectively and 'ax' is the lattice parameters values taken for calculations are:

R_1 for ZnSe Cubic Structure $- a_1 = 0.5576$ nm

R_2 for ZnTe Cubic Structure $- a_2 = 0.6084$ nm

and F_1 and F_2 are the molecular fraction of ZnSe and ZnTe respectively and

for ZnSe: $- F_1 = (1 - x) = 0.8, 0.6, 0.4, 0.2$

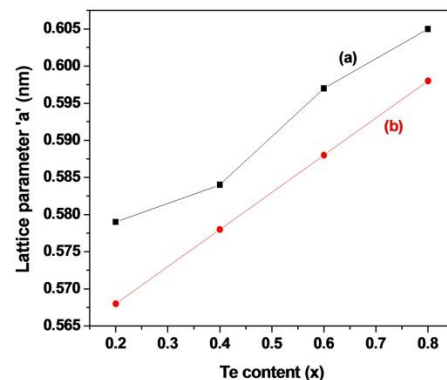for ZnTe: $- F_2 = x = 0.2, 0.4, 0.6, 0.8$

Fig. 3 – Lattice parameters of $ZnSe_{1-x}Te_x$ films as a function

Table 1 – Lattice parameters from XRD spectra of $ZnSe_{1-x}Te_x$ films

$ZnSe_{1-x}Te_x$ film	[hkl]	2θ (deg)	Lattice parameter 'a' (nm)	Calculated using equation 'R'
$ZnSe_{0.8}Te_{0.2}$	(111)	26.51	0.579	1.631
$ZnSe_{0.6}Te_{0.4}$	(111)	26.23	0.584	1.651
$ZnSe_{0.4}Te_{0.6}$	(111)	25.71	0.597	1.711
$ZnSe_{0.2}Te_{0.8}$	(111)	25.46	0.605	1.713

Table 2 – Microstructural parameters of $ZnSe_{1-x}Te_x$ solid solutions

Compositions	Grain size D nm	Strain $\varepsilon \times 10^{-4}$	Dislocation density $\delta \times 10^{18}$ line^2/cm^2	Stress S $\times 10^{10}$ dyne/cm^2	No. of Crystallites
$ZnSe_{0.8}Te_{0.2}$	10.9	0.292	9.21×10^{15}	-8.31×10^9	9.11×10^{16}
$ZnSe_{0.6}Te_{0.4}$	14.2	0.191	7.94×10^{15}	-6.47×10^9	4.21×10^{16}
$ZnSe_{0.4}Te_{0.6}$	17.7	0.116	1.68×10^{15}	-4.5×10^9	3.22×10^{16}
$ZnSe_{0.2}Te_{0.6}$	28.9	0.0718	0.642×10^{15}	-3.2×10^9	1.16×10^{16}

3.3 SEM studies of $ZnSe_{1-x}Te_x$ films

Surface morphology of $ZnSe_{1-x}Te_x$ thin films deposited by EB technique is presented in Fig. 4. The pictures were recorded at a magnification of 50,000 which is essential to visualize the nano grained surfaces of these films. All the surfaces are found smooth and uniformly distributed with nano grains. The grain size values are found to be about 48, 76, 94 and 115 nm for $ZnSe_{1-x}Te_x$ films with tellurium content $x = 0.2$, 0.4, 0.6 and 0.8 respectively. The increase in grain size is due to the incorporation of higher Te content in the ZnSe matrix. It is also reflecting the fact that replacement of selenium (low atomic radios) with tellurium (high atomic radios) is effective which leads to larger grained films with higher Te content.
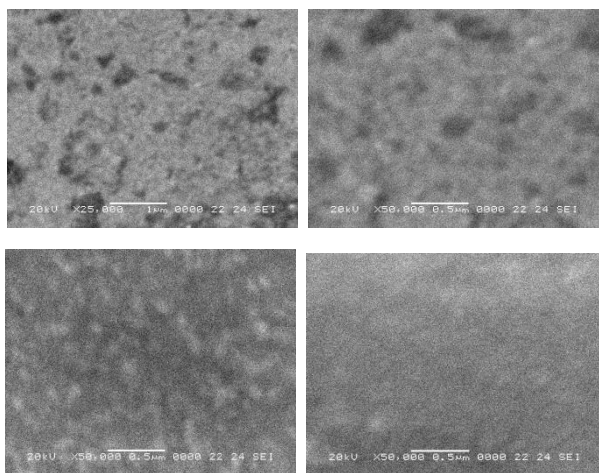

Fig. 4 – SEM pictures for the $ZnSe_{1-x}Te_x$ films with a) $x = 0.2$, b) $x = 0.4$, c) $x = 0.6$ and d) $x = 0.8$

3.4 AFM solutions of $ZnSe_{1-x}Te_x$ solid solutions

Atomic force microscope pictures of thin films surface give the three dimensional (3D) arrangement of grains and their arrangement. Two dimensional (2D) pictures give the surface quality with smoothness information and also provide the grain size calculation from a linear scan curve across the surface.

Fig. 5 a, b, c and d shows the 3D pictures of $ZnSe_{1-x}Te_x$ films with $x = 0.2$, 0.4, 0.6 and 0.8 respectively. The overall surface quality is very good without any pin holes or discontinuities. The grains are appearing globular sharp and uniformly distributed over the scanned area of 2 μm × 2 μm. The grain size is increasing with enhanced Te content in the film.
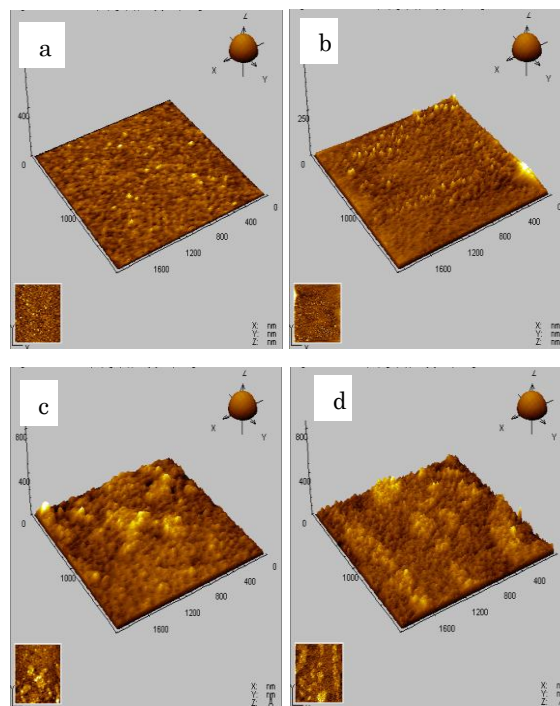

Fig. 5 – Three dimensional (3D) topographic AFM pictures for the $ZnSe_{1-x}Te_x$ films with a) $x = 0.2$, b) $x = 0.4$, c) $x = 0.6$ and d) $x = 0.8$

To have a close analysis of the film surface, 2D AFM pictures were recorded and are given in Fig. 6 a, b, c and d for the solid solution films with tellurium content x = 0.2, 0.4, 0.6 and 0.8 respectively. It is explicitly observed that the grain size is increasing with increasing tellurium content.

This is obviously due to the accepted fact that an atomic radio of Te is larger than the radios of Se. The $ZnSe_{1-x}Te_x$ films, prepared in the present study,

of form excellent solid solutions as explicitly seen from these AFM pictures. This reveals that there is one to one replacement of Se with Te atom in the crystal lattice.

This will reasonably reduce the dimension of the lattice leading to the formation of increased grain size when ZnSe is mixed with various amount of ZnTe. Along with 2D pictures, there is also given the line scan of the surface profile of each film.

The root mean square Roughness value was calculated from these line profile which is about 4.5, 5.2, 5.8 and 7.6 nm for the films with x = 0.2, 0.4, 0.6 and 0.8 respectively. Such a low R_{rms} value envisages the formation of nano crystalline $ZnSe_{1-x}Te_x$ films using EB evaporation technique.

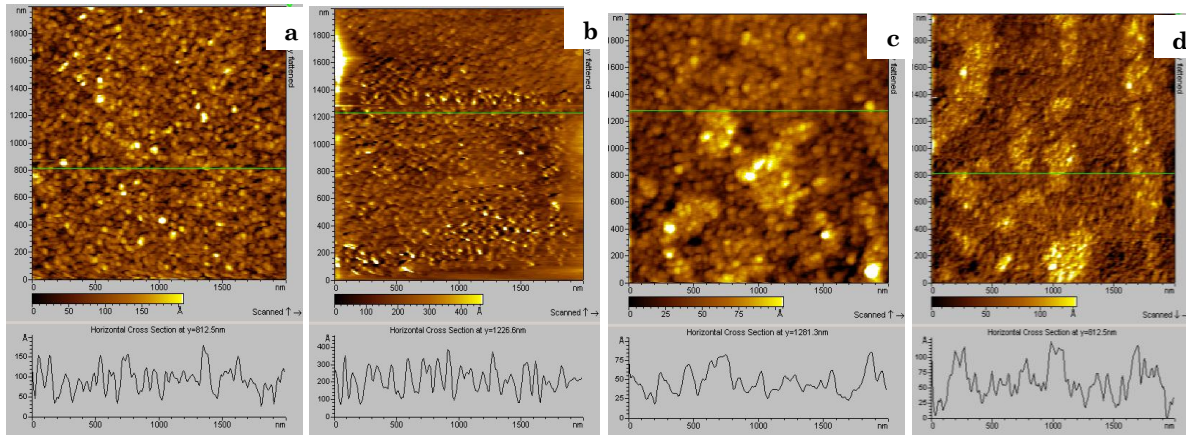**Fig. 6** – Two dimensional (2D) topographic AFM pictures for the $ZnSe_{1-x}Te_x$ films with a) $x = 0.2$, b) $x = 0.4$, c) $x = 0.6$ and d) $x = 0.8$

3.5 Raman spectral studies of ZnSe₁₋ₓTeₓ solid solutions

Raman scattering spectral studies were conducted for the solid solutions of $ZnSe_{1-x}Te_x$ films with x = 0.2, 0.4, 0.6 and 0.8. This is an important technique for analyzing the atomic distribution in the lattice of any structure. The effect of Te incorporation may be elegantly recognized by the Raman studies of these films with different Te content. $ZnSe_{1-x}Te_x$ films have been deposited by EB technique by keeping the substrate temperature constant at 200°C and the thickness also constant at about 200 nm.

It is interesting to note that the Raman spectra of these films show well-defined phonon peaks for the whole range of Te content as can be seen from Fig. 7. The observed Raman peak at 240.2 cm⁻¹ for the film with 0.2 Te content corresponds to the longitudinal (LO) phonon mode. This is the shifted LO mode of ZnSe Raman peak at 246.3 cm⁻¹. Similarly, this LO peak is found shifter to further low frequency side when the Te is increased to 0.4, 0.6 and 0.8 as seen in Fig. 7 b, c and d respectively. The observed phonon peak frequency value is 231.6, 224.4 and 218.2 cm⁻¹ respectively. The film with Te content equal to 0.8 shows the peak frequency value close to that of ZnTe films, 206.9 cm⁻¹.
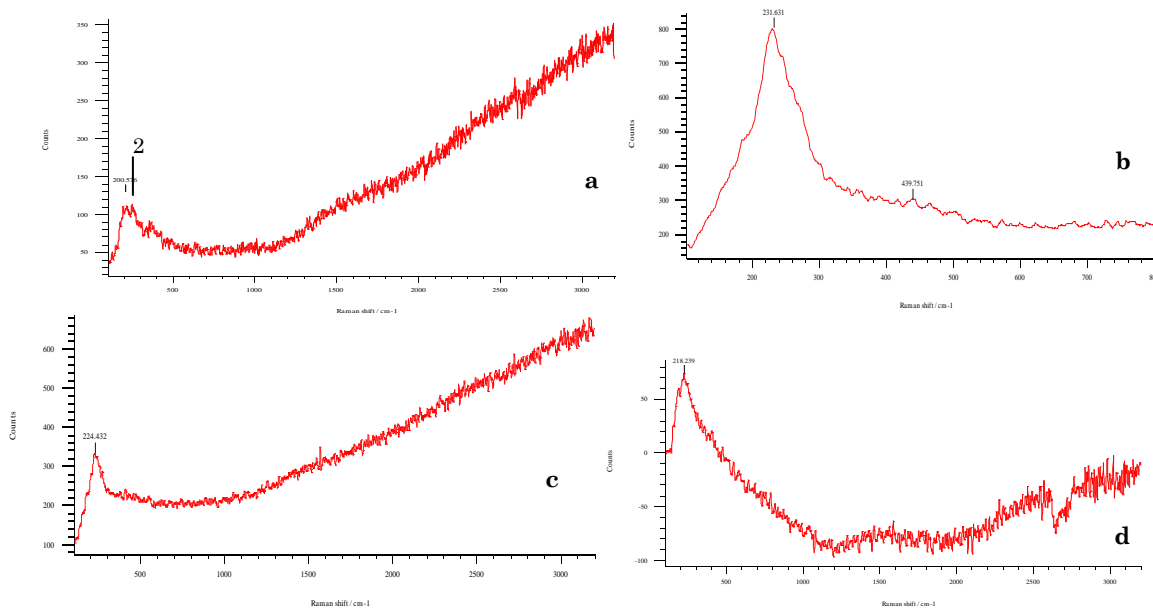

Fig. 7 – Raman spectra for the $ZnSe_{1-x}Te_x$ films with a) $x = 0.2$, b) $x = 0.4$, c) $x = 0.6$ and d) $x = 0.8$

Such a dependence of Raman peak on the Te content in the ZnSe$_{1-x}$Te$_x$ solid solutions has been reported only for the films deposited by molecular beam epitaxi (MBE) technique [18]. They have observed the phonon frequencies at about 243, 233, 222 and 216 cm^{-1} for their ZnSe$_{1-x}$Te$_x$ mixed crystals with tellurium content x = 0.2, 0.4, 0.6 and 0.8 respectively. Our Raman results are in very good agreement with these results. These variations are given in Fig. 8 a and b respectively. It confirms that EB evaporated ZnSe$_{1-x}$Te$_x$ films deposited in the present work are having mixed crystalline nature and make very good solid solutions which will help in making opto-electronic devices for varied applications.
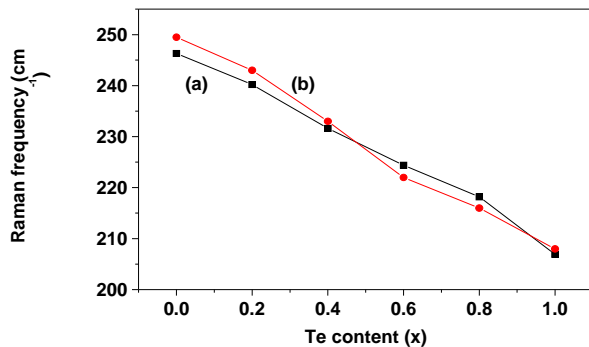

Fig. 8 – Variation of Raman frequency with Te content (*x*)

Such a dependence of Raman peak on the Te content in the ZnSe$_{1-x}$Te$_x$ solid solutions has been reported

only for the films deposited by molecular beam epitaxi (MBE) technique [18]. They have observed the phonon frequencies at about 243, 233, 222 and 216 cm^{-1} for their ZnSe$_{1-x}$Te$_x$ mixed crystals with tellurium content x = 0.2, 0.4, 0.6 and 0.8 respectively. Our Raman results are in very good agreement with these results. These variations are given in Fig. 8 a and b respectively. It confirms that EB evaporated ZnSe$_{1-x}$Te$_x$ films deposited in the present work are having mixed crystalline nature and make very good solid solutions which will help in making opto-electronic devices for varied applications.

4. CONCLUSION

The solid solutions of ZnSe and ZnTe binary compounds have been deposited on glass substrates through EB evaporation route. XRD studies showed continuous variation in 'a' values confirming the solid solution formation. Optical studies showed band gap decrease with Te content and very low bowing parameters confirms the Vegards' law. Optical vibrational studies by Raman and FTIR show the formation of ZnSe$_{1-x}$Te$_x$ solid solutions. Surface morphological studies by SEM and AFM show uniform surface with globular grains. The resistivity values may be very high owing to the formation of larger zinc vacancies in the crystal lattice.

REFERENCES

1. I.V. Akimova, A.M. Akhekyan, V.I. Kozolovsky, Yu.V. Korostelin, and P.V. Shapin, Sov. *Phys. Solid State* **27**, 1041 (1985).
2. S. Permogorov and A. Reznitsky, *J. Lumin.* **52**, 201 (1992).
3. I.L. Kuskovsky, C. Lin, S.P. Guo, and M.C. Tamargo, *Phys. Rev. B* **63**, 155205 (2001).
4. K. Suzuki, U. Neukirch, J. Gutowski, N. Takojima, T. Sawada, and K. Imai, *J. Crystal Growth* **184/185**, 882 (1998).
5. M.C. Kuo, C.S. Yang, P.Y. Tseng, J. Lee, J.L. Shen, W.C. Chou, Y.T. Shih, C.T. Ku, M.C. Lee and W.K.J. Chen, *J. Crystal Growth* **242**, 533 .
6. S.H. Wei and A. Zunger, *Phys. Rev.* **457** B 53, R10 (1996).
7. W.L. Wang, *Phys. Rev.* B **63**, (2001) 245107.
8. E.R. Glaser, B.R. Bennett, B.V. Shanabrook, and R. Magno, *Appl. Phys. Lett*. **68**, (1996) 3614.
9. K. Naniwae, H. Iwata, N. Kukoda, K. Yashiki, M. Kuramoto, K. Gomyo and T. Suzuki, in: *Proc. of the Int. Symp. on Blue laser and Light Emitting Diodes*, **86**, 1996.
10. Y.M. Yu, S. Nam, J.K. Rhee, O. Byungsung, K.S. Lee, Y.D. Choi, *J. Crystal Growth*, **210** 521 (2000).
11. J.E. Bernard, A. Zunger, *Phys. Rev. B* **34** 5992 (1986).
12. L.A. Farrow, J.M. Worlck, F. Turco-Sandroff, R.E. Nahory, R. Beserman, D.M. Hwang, *Phys. Rev. B* **45**, 1231 (1992).
13. L. Genzel, T.P. Martin, C.H. Perry, *phys. status. solidi B* **62**, 83 (1974).
14. K. Dhese, J.E. Nicholls, J. Goodwin, W.E. Hagston, J.J. Davies, M.P. Halsall, B. Cockayne, P.J. Wright, *J. Crystal Growth* **117,** 91 (1992).
15. M. Prutton, *Surface Physics*, Oxford University Press, Oxford, 1975. (**Chapter 6**).
16. F.S. Turco-Sandroff, R.E. Nahory, M.J.S.P. Brasil, R.J. Martin, R. Beserman, L.A. Farrow, J.M. Worlock, A.L. Weaver, *J. Crystal Growth* **111**, 762 (1991).
17. J.C. Phillips, *Bonds and Bands in Semiconductors*, Academic Press, New York, 1973. (**Chapter 8**).
18. Avdonin, P. Gashin, D. Nedeoglo, N. Nedeoglo, V. Ryjikov, V. Sirkeli, *Moldavian Journal of the Physical Sciences* **1**, 40 (2002).